J. Fluid Mech. (1974), *vol.* 66, *part* 1, *pp.* 115–143
Printed in Great Britain

Relaxation effects, caused by relative motion, on shock waves in gas-bubble/liquid mixtures

By L. NOORDZIJ
Netherlands Ship Model Basin Wageningen, The Netherlands
AND L. VAN WIJNGAARDEN
Twente Institute of Technology, Enschede, The Netherlands

(Received 29 December 1972 and in revised form 3 May 1974)

We observed a gradual change in the structure of a shock wave passing through a long tube of bubbly liquid, which we attribute to the motion of the bubbles relative to the liquid. We show that the effect of the motion on the structure of a shock wave is like that of thermal relaxation on gasdynamic shock waves: the pertinent relaxation time is the time viscous forces in the fluid take to alter the velocity of a bubble to that of the fluid. Our theory predicts certain changes in the speed of the shock wave and in its structure. We could not verify the prediction as to wave speed: in dilute mixtures it is too small to be measured. But we report experiments on the structure of the wave, which support our theoretical conclusion that the observed changes are due to the relative motion.

1. Introduction

This paper deals with shock waves in a mixture of a liquid and small gas bubbles. Campbell & Pitcher (1958), among the first to investigate this subject, derived Hugoniot relations, and experimentally verified the deduced relation between shock strength and velocity of propagation. Later theoretical work on shock waves of moderate amplitude (Crespo 1969; van Wijngaarden 1970) showed that they are governed by equations of the same type as those for long gravity waves on water of finite depth, which suggested that the pressure profile of a stationary wave looks like the surface elevation of an undular bore. The investigations of Noordzij (1973) and van Wijngaarden (1972*b*) tended to confirm this. Their experiments were carried out in a shock tube about 1 m long. Subsequently we built a longer tube, and observed that the wave (which perfectly resembled an undular bore in the first part of the tube) changed form in a way not to be explained by existing theory. (Schematic of tube, figure 1; description of the apparatus, §6.)

The profile of a pressure wave passing along the tube was recorded at three locations (*A*, *B* and *C* in figure 1). *A* is 0·20 m from the top, *B* at 2·5 m and *C* at 4 m. We present these profiles and other experimental data in §6. In figure 2 (plate 1), we show as an illustration the change in form of the profile of a wave with an initial pressure ratio 1·08, propagating through a mixture with a mean

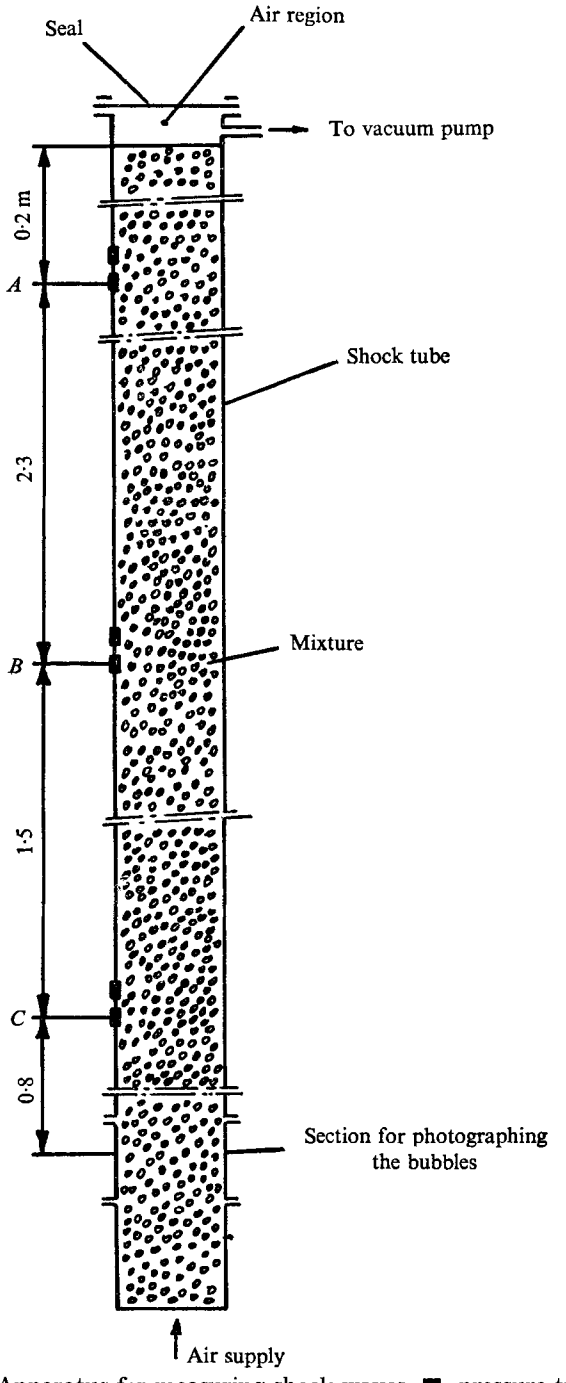

FIGURE 1. Apparatus for measuring shock waves. ■, pressure transducer.

gas concentration by volume of 2·9 %, the bubbles having an initial radius of 1·1 mm. At A the present profile has the form typical of an undular bore: a steep rise in pressure at the front and waves at the back. At B the steep rise at the front is still there, but the pressure no longer rises to the equilibrium pressure at the back. This takes place in a region, much thicker than the front shock, in which, slowly oscillating, the pressure reaches its final value. In C the front shock and the oscillations disappear; the pressure profile is almost completely smooth; and it covers a region at least an order of magnitude greater than the thickness of the front shock in A.

This change in profile cannot be explained by the theory of van Wijngaarden (1970), which is based on the idea that there is a balance in the wave between the tendency to steepen (due to nonlinear effects) and to spread out (due to linear dispersion). The balance is realized in A (figure 2, plate 1), where the thickness and other typical properties of the wave agree very satisfactorily with the earlier theory. To find why the B and C profiles develop we took a close look at effects neglected in the earlier theory, and concluded that they stem from the motion of the bubbles relative to the liquid. After a typical time τ, initial relative motion (produced e.g. by a step wave) is resisted by a viscous force proportional to the relative velocity. Similar 'rate' processes occur in gasdynamic shocks: their ('relaxation') effects on shocks are well understood in gasdynamics (Lighthill 1956; Whitham 1959; Ockendon & Spence 1969). Of great importance in drawing the analogy with gasdynamics is how to describe the relative motion with sufficient accuracy. To solve this problem, we use the theory introduced by Levich (1962) for spherical bubbles, and extended by Moore (1965) for oblate ellipsoids. Sections 2–5 deal with the resulting theory of *relaxation shocks in bubbly suspensions.*

2. Equations of motion

We consider a time-dependent flow, in the x direction, of a dilute mixture of spherical gas bubbles with liquid. When there are n bubbles in a unit volume of the mixture, and locally these all have a radius R, the ratio between inter-bubble distance and bubble size is proportional to $(n^{\frac{1}{3}}R)^{-1}$. We deal with mixtures in which this ratio is large compared with unity, which means that the volume of gas in a unit volume of the mixture β is small, since

$$\beta = \tfrac{4}{3}\pi n R^3. \tag{2.1}$$

The mass densities of fluid and gas are ρ_f and ρ_g, respectively; that of the mixture is ρ. The contribution to ρ by ρ_g can safely be neglected, so

$$\rho = \rho_f(1-\beta). \tag{2.2}$$

Sometimes we shall use concentration by mass α/ρ_f (i.e. the volume of gas in a unit mass of the mixture) instead of β:

$$\alpha = \beta/(1-\beta). \tag{2.3}$$

u is the continuum liquid velocity (the average velocity over a volume element

which is small compared with the apparatus, yet contains many bubbles). The equation of mass conservation is

$$\frac{\partial \rho}{\partial t} + \frac{\partial}{\partial x}(\rho u) = 0. \tag{2.4}$$

Our definition of the liquid pressure p is analogous to our definition of u; the momentum equation is thus

$$\frac{\partial}{\partial t}\rho u + \frac{\partial}{\partial x}(p + \rho u^2) = 0. \tag{2.5}$$

The velocity of a bubble is v.

There are several reasons why the pressure of the gas in the bubbles p_g may differ from p. (i) The inertia of the liquid accelerated or decelerated with respect to the bubble–liquid interface, in the radial direction. This inertia causes dispersion of pressure waves. (ii) Further, surface tension may cause a difference between the pressure inside a bubble and that outside. The coefficient of surface tension σ is here of order 10^{-1}, the pressure p_g is atmospheric and the bubble radius is of order 10^{-3}, which makes σ/R negligible. (iii) There are various damping mechanisms, the most important being heat conduction from the fluid into the gas, and vice versa.

In a universally valid expression for $p - p_g$, these effects are represented by strongly nonlinear terms. But, for waves of moderate amplitude, we may restrict ourselves to an expression for $p - p_g$ valid for acoustic waves (see van Wijngaarden 1968). With R_0 the undisturbed bubble radius, this relation is

$$\frac{p_g - p}{\rho_f R_0^2} = \frac{\partial^2}{\partial t^2}(R/R_0) + \delta\omega_B \frac{\partial}{\partial t}(R/R_0). \tag{2.6}$$

In (2.6) the bubble resonance frequency

$$\omega_B = [3p_0/(\rho_f R_0^2)]^{\frac{1}{2}}, \tag{2.7}$$

and δ is the sum of the contributions δ_{v}, δ_{th} and δ_{ac} from viscous dissipation, heat conduction and acoustic radiation (due to the finite velocity of sound in the liquid c_l), respectively. For a mixture in which the liquid has a kinematic viscosity ν and the gas a ratio of specific heats γ,

$$\delta_{\mathrm{v}} = 4\nu/(\omega_B R_0^2), \quad \delta_{\mathrm{ac}} = \gamma\omega_B R_0/c_l, \quad \delta_{\mathrm{th}} = 4{\cdot}41 \times 10^{-4}(\gamma\omega_B/2\pi)^{\frac{1}{2}} \tag{2.8}$$

(see e.g. van Wijngaarden 1972*a*). We neglect the small effect of relative translational motion on the dispersion equation (2.6). When $v - u = 0$, the mass of gas in a unit mass of the mixture is constant. Since $p_g \sim \rho_g$, this means that

$$p_g \alpha = \text{const.} = p_0 \alpha_0,$$

where the subscript 0 refers to the undisturbed state. Together with $p_g R^3 = p_0 R_0^3$ (the isothermal relation), and the expression for the speed of sound (see van Wijngaarden 1972*a*)

$$c_0^2 = \frac{p_0(1 + 2\alpha_0)}{\rho_f \alpha_0}, \tag{2.9}$$

this enables us to write (2.6) as

$$\frac{p_g - p}{p_0} = \frac{R_0^2}{3\alpha_0^2 c_0^2}\left\{\frac{\partial^2 \alpha}{\partial t^2} + \delta\omega_B \frac{\partial \alpha}{\partial t}\right\}. \tag{2.10}$$

Incidentally, when inertial effects are negligible and we set $\delta = \delta_v$, (2.6) may be written as

$$p_g - p = \frac{4\mu}{3\alpha_0}\frac{\partial u}{\partial x},$$

with $\mu = \rho_f \nu$, indicating that viscous stresses associated with radial motion give the mixture an apparent bulk viscosity of $4\mu/(3\alpha)$ (Taylor 1954). Equation (2.7) supposes the gas to be isothermal.

We shall consider both adiabatic and isothermal behaviour, though the liquid is assumed isothermal, because its heat capacity is very large compared with that of the gas. (For the present, we treat changes of volume of the bubbles as isothermal; in § 5 we give the pertinent adiabatic results.) For a bubble of volume V, $p_g V$ is constant during isothermal changes. Using (2.1) and the expression for the conservation of the number density n (breaking up or dissolution of bubbles is excluded)

$$\frac{\partial n}{\partial t} + \frac{\partial}{\partial x}(nv) = 0, \tag{2.11}$$

this gives

$$\frac{\partial}{\partial t}(p_g \beta) + \frac{\partial}{\partial x}(p_g v \beta) = 0. \tag{2.12}$$

Our most important task is to give a sufficiently accurate description of the dynamics of the motion of the bubbles relative to the liquid. When surface-active agents are absent, and the Reynolds number

$$Re = [2(v-u)R]/\nu \tag{2.13}$$

is large compared with unity, the flow around the bubble is very nearly potential, because there is no boundary layer for the velocity. A boundary layer does exist for the velocity gradient, just as at the free surface of gravity waves; but neglect of this is justified in a first approximation (see Levich 1962; Moore 1963, 1965). Dissipation takes place in the potential flow around the bubble; and it can be calculated from the potential. For a spherical bubble, Levich (1962) and Moore (1963) thus obtained the viscous drag

$$D = 12\pi\mu R(v-u). \tag{2.14}$$

This relation holds for both unsteady and steady flow, because it follows from potential flow, which is established instantaneously. For steady flow, Moore (1963) also calculated the effect of the boundary layer for the velocity gradient, and he obtained the drag coefficient

$$C_D = \frac{48}{Re}\left(1 - \frac{2{\cdot}2}{Re^{\frac{1}{2}}}\right). \tag{2.15}$$

The second term on the right-hand side estimates the error involved in using (2.14) at finite Re. The Levich formula (2.14) presupposes a spherical bubble;

and in the shock waves we are concerned with, the bubbles may not be always spherical; so we have to take possible deformation into account. A measure for the deformation is the Weber number

$$We = [2\rho_f(u-v)^2 R]/\sigma \tag{2.16}$$

(R is the effective bubble radius, σ the coefficient of surface tension).

For $We < 1$, (2.14) gives the drag on a bubble. The Weber numbers for which Moore (1965) calculated the drag are not small, yet they are of unit order (1–4, say). Moore calculated the drag as a function of We and the axis ratio χ (of the major to the minor axis) of the oblate ellipsoid the bubbles deform to:

$$We = 4\chi^{-\frac{4}{3}}(\chi^3+\chi-2)\{\chi^2\sec^{-1}\chi-(\chi^2-1)^{\frac{1}{2}}\}^2(\chi^2-1)^{-3}. \tag{2.17}$$

We is restricted to about 4, because Moore could find no equilibrium ellipsoid above that value. For given χ, Moore calculated that the drag

$$D = 12\pi\mu R(v-u)\,G(\chi), \tag{2.18}$$

where

$$G(\chi) = \tfrac{4}{3}(\chi^2+\chi-2)\,[(\chi^2-1)^{\frac{1}{2}}-(2-\chi^2)\sec^{-1}\chi]\,[We(\chi^2-1)^{\frac{3}{2}}]^{-1}. \tag{2.19}$$

$D = 1$ when $\chi = 1$, and rises rather steeply with χ. In a number of our experiments We exceeded unity, making it necessary to use (2.18) (see §6). Since the phenomena in shock waves are unsteady, finite Re corrections like these in (2.15), or similar corrections for oblate ellipsoids (also in Moore 1965) cannot be applied. The equation of motion for a single bubble may now be written down. This must capture the fact that the rate of change of impulse (see Lamb 1932, §119) $m(v-u)$ equals the sum of the drag and the force $-V\,\partial p/\partial x$ arising from the pressure gradient in the external flow. The virtual mass m is $\frac{1}{2}\rho_f V$ for a sphere, and increases with the axis ratio χ for an oblate ellipsoid. The pertinent relation between χ and m is given in Milne-Thomson (1968) in the following way. Write

$$m = \tfrac{1}{2}\rho_f V O(\chi). \tag{2.20}$$

Hence

$$Q(\chi) = 2\frac{(\chi^2-1)^{\frac{1}{2}}-\cos^{-1}\chi^{-1}}{\cos^{-1}\chi^{-1}-(\chi^2-1)^{\frac{1}{2}}/\chi^2}. \tag{2.21}$$

When R is understood as the effective bubble radius, the equation of motion becomes, with drag force and added mass in terms of (2.18) and (2.20),

$$\frac{d}{dt}\{\tfrac{1}{2}\rho_f VQ(v-u)\} = -V\frac{\partial p}{\partial x} - 12\pi\mu R(v-u)\,G. \tag{2.22}$$

Using the definition of β, (2.1), and the conservation of bubbles, (2.11), this gives, at small values of β that permit the neglect of convective acceleration,

$$\frac{\partial}{\partial t}\{\beta(v-u)\,Q\} + 24\pi\nu nRG(v-u) = -\frac{2\beta}{\rho_f}\frac{\partial p}{\partial x}.$$

For the moderate pressure changes we have in mind, a further approximation may be made by writing nR as nR^3/R_0^2, which results in

$$\frac{\partial}{\partial t}\{\beta(v-u)\,Q\} + \frac{18\nu}{R_0^2}(v-u)\,G = -\frac{2\beta}{\rho_f}\frac{\partial p}{\partial x}. \tag{2.23}$$

Equation (2.23) will be used for the relative velocity $v-u$. It describes a relaxation process with a relaxation time which can easily be determined for a spherical bubble for which both G and Q equal unity. Then we can define a relaxation time

$$\tau' = R_0^2/(18\nu); \tag{2.24}$$

and the relaxation equation is

$$\left(\frac{\partial}{\partial t}+\tau'^{-1}\right)\{\beta(v-u)\} = -\frac{2\beta}{\rho_f}\frac{\partial p}{\partial x}. \tag{2.25}$$

At times t such that $t \ll \tau'$, relative motion is not resisted by viscous friction, which becomes effective for times comparable with and larger than τ'. Provided the driving force $\partial p/\partial x$ eventually tends to zero, ultimately relative motion vanishes.

For deformed bubbles, no simple equation like (2.25) can be given for all times t. Section 4 deals with two typical situations. In the first, viscous friction is unimportant. Then, from (2.23),

$$\frac{\partial}{\partial t}\{\beta(v-u)\,Q\} = -\frac{2\beta}{\rho_f}\frac{\partial p}{\partial x}. \tag{2.26}$$

This is applicable in part A (figure 1) of the shock tube (see §§ 3 and 4). Section 4 also deals with relaxation zones of large width, in which χ varies slowly. In this case we shall use a representative value χ^*, and define a representative relaxation time τ by

$$\tau = \frac{Q_*}{G_*}\frac{R_0^2}{18\nu}, \tag{2.27}$$

with obvious notation. Then (2.23) reduces to

$$\left(\frac{\partial}{\partial t}+\tau^{-1}\right)\{Q_*\beta(v-u)\} = -\frac{2\beta}{\rho_f}\frac{\partial p}{\partial x}. \tag{2.28}$$

For convenience, we now list the equations to be used in § 3:

$$\rho = \rho_f(1-\beta) = \frac{\rho_f}{1+\alpha}, \quad \alpha = \frac{\beta}{1-\beta} \simeq \beta(1+\beta), \tag{2.29), (2.30}$$

$$\frac{\partial \rho}{\partial t}+\frac{\partial}{\partial x}(\rho u) = 0, \quad \frac{\partial \rho u}{\partial t}+\frac{\partial}{\partial x}(p+\rho u^2) = 0, \tag{2.31), (2.32}$$

$$\frac{\partial}{\partial t}(p_g\beta)+\frac{\partial}{\partial x}(p_g\beta v) = 0, \tag{2.33}$$

$$\frac{\partial}{\partial t}\{\beta(v-u)\,Q\}+\frac{18\nu}{R_0^2}(v-u)\,G = -\frac{2\beta}{\rho_f}\frac{\partial p}{\partial x}, \tag{2.34}$$

$$\frac{p_g-p}{p_0} = \frac{R_0^2}{3\alpha_0^2 c_0^2}\left\{\frac{\partial^2\alpha}{\partial t^2}+\delta\omega_B\frac{\partial \alpha}{\partial t}\right\}. \tag{2.35}$$

3. The effects of relative translational motion on wave propagation

The general features of compressive waves through mixtures, governed by (2.29)–(2.35), are known for the case when there is no relative motion (review in van Wijngaarden 1972*a*). For $\delta = 0$ and $\tau = 0$ (i.e. no dissipation or relative motion), with

$$\tilde{p} = (p_g - p_0)/p_0,$$

waves of moderate amplitude are governed by

$$\frac{\partial \tilde{p}}{\partial t} + c_0 \frac{\partial \tilde{p}}{\partial x} + c_0 \tilde{p} \frac{\partial \tilde{p}}{\partial x} + \frac{1}{2} \frac{c_0^3}{\omega_B^2} \frac{\partial^3 \tilde{p}}{\partial x^3} = 0, \tag{3.1}$$

an equation of the Korteweg–de Vries type, indicating the possible existence of cnoidal waves and bores. Solutions in the form of steady shock waves are obtained when dissipation is included; and (3.1) becomes

$$\frac{\partial \tilde{p}}{\partial t} + c_0 \frac{\partial \tilde{p}}{\partial x} + c_0 \tilde{p} \frac{\partial \tilde{p}}{\partial x} + \frac{1}{2} \frac{c_0^3}{\omega_B^2} \frac{\partial^3 \tilde{p}}{\partial x^3} - \frac{1}{2} \frac{\delta c_0^2}{\omega_B} \frac{\partial^2 \tilde{p}}{\partial x^2} = 0. \tag{3.2}$$

Shock waves with pressure profiles required by solutions of (3.2) were obtained by experiment (van Wijngaarden 1972*b*; Noordzij 1973).

The novel effect we investigate here is that of relative motion. From what is known in gasdynamics about the effect of 'rate processes' as described by (2.34) (Lighthill 1956; Whitham 1959; Ockendon & Spence 1969), much can be learned and directly used. Waves in dusty gases (where, in contrast to the mixture considered here, the continuum phase is compressible and the dispersed incompressible) provide another possibility for comparison; and some aspects (as reviewed by Marble 1970) are of interest here. So much of what follows can be anticipated from what is known in similar fields; but it is precisely the differences (such as the inertia associated with relative radial flow as described by (2.35), the specific form of (2.34)) that make analysis necessary for comparison with experiments (in §6).

We first restrict ourselves to the effect of relative motion, and we consider small-amplitude waves in a mixture where $p_g = p$. For this it is sufficient to concern ourselves with spherical bubbles, in which case the relaxation time τ' is given by (2.24).

Straightforward linearization of (2.31)–(2.34) reveals the existence of two characteristic speeds, because the resulting equations yield

$$\frac{\partial}{\partial t}\left\{c_f^2 \frac{\partial^2 \tilde{p}}{\partial x^2} - \frac{\partial^2 \tilde{p}}{\partial t^2}\right\} + \tau'^{-1}\left\{c_0^2 \frac{\partial^2 \tilde{p}}{\partial x^2} - \frac{\partial^2 \tilde{p}}{\partial t^2}\right\} = 0. \tag{3.3}$$

The speed c_0 has been defined before; the speed

$$c_f = [c_0^2(1 + 2\beta_0)]^{\frac{1}{2}}. \tag{3.4}$$

This was found by Crespo (1969), who considered the case $\tau' \to \infty$; it is the speed of sound in a mixture where the relative motion is not resisted by friction. In this case the concentration of bubbles is locally less than it is when the bubbles

move with the fluid. This gives the mixture a greater stiffness, and consequently a sound velocity larger than c_0. The general features of solutions of (3.3) are well known: for times $t \ll \tau'$, the solutions represent waves propagating at speed c_f; for times $t \gg \tau'$, the waves propagate at c_0, and the motion is governed by the terms preceded by τ'^{-1} in (3.3). The higher-order terms have a diffusive effect on these waves. This follows, for example, by substituting in the equation valid for a wave which travels to the right,

$$\frac{\partial}{\partial t}\left(c_f \frac{\partial \tilde{p}}{\partial x} + \frac{\partial \tilde{p}}{\partial t}\right) + \tau'^{-1}\left(c_0 \frac{\partial \tilde{p}}{\partial x} + \frac{\partial \tilde{p}}{\partial t}\right) = 0, \tag{3.5}$$

$-c_0 \partial/\partial x$ for $\partial/\partial t$ in the first and second term on the left-hand side, resulting in

$$\frac{\partial \tilde{p}}{\partial t} + c_0 \frac{\partial \tilde{p}}{\partial x} - \tau'(c_f^2 - c_0^2)\frac{\partial^2 \tilde{p}}{\partial x^2} = 0. \tag{3.6}$$

Wave-type solutions of (3.6) represent waves travelling at speed c_0 and diffused by the action of the third term on the left-hand side. The diffusion coefficient is $\tau'(c_f^2 - c_0^2)$. In waves of finite amplitude, diffusion may be resisted by nonlinear effects, comparable with the role of thermodynamic relaxation in gasdynamic waves (see e.g. Lighthill 1956; Whitham 1959; Ockendon & Spence 1969).

To see how in our case relaxation, dissipation, dispersion and nonlinearity work together (or oppose each other), we write

$$p = p_0(1 + \epsilon p'), \quad \beta = \beta_0(1 + \epsilon\beta'), \quad u = \epsilon c_0 u', \quad v = \epsilon c_0 v', \quad \text{etc.}$$

The subscript 0 refers to the undisturbed state. This is introduced in (2.29)–(2.35). Terms of order ϵ^2 and lower are retained; terms of order $\epsilon^2\beta_0$ are discarded. We omit details, and merely state the result: omitting the primes, for a wave in positive x direction,

$$\frac{\partial}{\partial t}\left\{c_f \frac{\partial p}{\partial x} + \frac{\partial p}{\partial t} + c_f \epsilon p \frac{\partial p}{\partial x} + \frac{c_f^3}{2\omega_B^2}\frac{\partial^3 p}{\partial x^3} - \frac{\delta c_f^2}{2\omega_B}\frac{\partial^2 p}{\partial x^2}\right\}$$
$$+ \tau'^{-1}\left\{c_0 \frac{\partial p}{\partial x} + \frac{\partial p}{\partial t} + c_0 \epsilon p \frac{\partial p}{\partial x} + \frac{c_0^3}{2\omega_B^2}\frac{\partial^3 p}{\partial x^3} - \frac{\delta c_0^2}{2\omega_B}\frac{\partial^2 p}{\partial x^2}\right\} = 0. \tag{3.7}$$

Once (3.2), which does not take relaxation into account, and (3.5), which takes only this effect into account, are known, (3.7) is to be expected, because it is well known that, in an approximation one order beyond the linear, the various effects can simply be added in the resulting equation, provided the effects of dispersion, relaxation and dissipation are small. In terms corresponding to these effects, as well as in nonlinear terms, it is immaterial whether c_f or c_0 appears, because the difference between them is of order β_0. To preserve symmetry, we have introduced c_f into these terms in the first line of (3.7), c_0 in the second. Equation (3.7) is of the type discussed in Whitham (1959), in particular for an initial profile in the form of a Heaviside step function (as is the case in our shock tube experiments). For times $t \ll \tau'$, the second line in (3.7) can be left out and the wave is governed by (3.2), but with c_f in place of c_0. Since τ' is of order 10^{-2} s and c_f of order $10^2\,\mathrm{m\,s^{-1}}$, the relaxation process becomes effective after the wave has

travelled several metres. Numerical computations on (3.2) showed that the solution does not change appreciably after travelling a couple of centimetres. We may therefore assume that the wave form, as observed in section A of the shock tube in figure 1, represents the steady solution of (3.2) (with c_f instead of c_0).

After the wave has propagated over a distance of order $c_f\tau'$, the relaxation mechanism becomes important. Its effect on the wave is, as we have seen, diffusive. In an acoustic wave, this diffusion is not resisted, and the wave ultimately diffuses out. In a nonlinear wave, however, the diffusion is resisted by nonlinear steepening, and a steady profile is possible in which these mechanisms exactly balance. This can only occur when the strength of the shock is less than a certain critical value, which can be calculated with help of Lighthill (1956). The argument is this. The wave travels steadily at a speed U which is, for our waves (see e.g. van Wijngaarden 1970) related to c_0 by $U/c_0 = (p_1/p_0)^{\frac{1}{2}}$, where p_1 is the pressure behind the wave. On the other hand, if the profile is smooth, the wavelets at the front travel with speed at most c_f, related to c_0 by $c_f = c_0(1+\beta_0)$ (cf. (3.4)). Since the wave is steady, the speed of the front equals U, whence

$$p_1/p_0 \leqslant 1+2\beta_0. \tag{3.8}$$

To this class of profiles belongs that observed in section C of the shock tube, and shown in figure 2 (plate 1). The thickness d_C of these waves can be estimated using $c_0\tilde{p}(\partial\tilde{p}/\partial x)$ and the diffusion term $\tau'(c_f^2-c_0^2)\,(\partial^2\tilde{p}/\partial x^2)$ in (3.6), which must be of equal magnitude in these waves. It follows that

$$d_C \simeq \frac{\tau' c_0(c_f^2/c_0^2-1)}{p_1/p_0-1}; \tag{3.9}$$

(3.8) indicates that this is of the order of one metre. In A the nonlinear term must balance with the dispersion term; so

$$d_A \simeq \frac{R_0}{\beta_0^{\frac{1}{2}}(p_1/p_0-1)^{\frac{1}{2}}}, \tag{3.10}$$

which amounts to a few centimetres for not too weak shocks (see Noordzij 1973). When p_1/p_0 exceeds $1+2\beta_0$, no completely smooth profile is possible; and Whitham (1959) shows that the wave resisted by diffusion is preceded by a thin shock of the same sort as the front in A. The strength p^*/p_0 of this shock can be calculated (as in § 4) from Hugoniot relations. This is the type of wave (in B in figure 2) where a thin region (of order of magnitude given by (3.10)) is followed by a much thicker region (with thickness as in (3.9)).

The discussion of § 3 serves to explain the occurrence of different types of shock profiles as the shock travels down the tube. These profiles are all steady in an appropriate sense. In § 4 we shall deal with the profiles in more detail to obtain results on shock speed, thickness and other characteristic properties that may be compared with measurement.

4. Structure of steady shock waves

We consider a shock wave moving with constant speed U in the negative x direction. Equations (2.31)–(2.35) are written in the independent variables x and t. We transform these into x', t, where $x' = x+Ut$. In this new frame, the

shock wave is steady, and $(\partial/\partial t)_{x'}$ therefore zero. Carrying out this transformation on (2.31), we obtain, after integration, the upstream conditions indicated with subscript 0:

$$\rho_f(1-\beta)(U+u) = \rho_f(1-\beta_0)U. \tag{4.1}$$

The shock-induced velocity is, as follows from (2.30) and (4.1),

$$u = \beta_0 U(\alpha/\alpha_0 - 1). \tag{4.2}$$

Likewise, the momentum equation becomes

$$p_0 = p + \rho_f(1-\beta_0)Uu. \tag{4.3}$$

Substitution of (4.2) into (4.3) gives, with help of (2.30) and the expression (2.9) for the sound speed c_0,

$$\frac{p}{p_0} - 1 = \frac{U^2}{c_0^2}\left(1 - \frac{\alpha}{\alpha_0}\right). \tag{4.4}$$

The analysis is, from here on, different for the various types of steady shocks we associated with parts A, B and C respectively in the shock tube of figure 1. We call these three types for convenience A, B and C shocks.

A shocks

Here relative motion is not yet resisted by friction, and we can use (2.26) for the relative acceleration. Expressing p in terms of α with (4.4) and replacing $\partial/\partial t$ by $U\,d/dx$, we find upon integration, omitting terms of order α^3,

$$\alpha Q(v-u)/U = \alpha^2 - \alpha_0^2. \tag{4.5}$$

It is assumed that $v = u = 0$ ahead of the shock (i.e. we neglect the relative velocity caused by buoyancy). This is small in our experiments compared with the shock-induced velocity; and it is of opposite sign, because the shocks travel in a direction opposite to gravity. In a frame moving with the shock, (2.33) becomes

$$\frac{p_g}{p_0} = \frac{\beta_0 U}{\beta(v-u) + \beta(u+U)}. \tag{4.6}$$

With the help of (2.30), (4.2) and (4.5), this is, in terms of α,

$$\frac{p_g}{p_0} = \frac{\alpha_0}{\alpha}\{1 - (Q\alpha)^{-1}(\alpha^2 - \alpha_0^2)\}.$$

Together, with (4.4), this leads to

$$\frac{p_g - p}{p_0} = \frac{(\alpha_0 - \alpha)(\alpha_0 - U^2\alpha/c_0^2)}{\alpha\alpha_0} - \frac{\alpha_0}{Q\alpha^2}(\alpha^2 - \alpha_0^2). \tag{4.7}$$

At the back of the shock, $x \to \infty$; where pertinent quantities are indicated with the subscript 1, $p_g = p = p_1$; whence, from (4.7),

$$\frac{(\alpha_0 - \alpha_1)(\alpha_0 - U^2\alpha_1/c_0^2)}{\alpha_1\alpha_0} - \frac{\alpha_0}{Q_1\alpha_1^2}(\alpha_1^2 - \alpha_0^2) = 0. \tag{4.8}$$

Further we have, from (4.4),

$$\frac{p_1}{p_0} - 1 = \frac{U^2}{c_0^2}\left(1 - \frac{\alpha_1}{\alpha_0}\right). \tag{4.9}$$

Eliminating α_1/α_0 using these expressions and neglecting terms of order α_0^2, we obtain, with (3.4),

$$\frac{U^2}{c_f^2} = \frac{p_1}{p_0}\left[1 - \alpha_0\left\{2 - Q_1^{-1}\left(1 + \frac{p_0}{p_1}\right)\right\}\right]. \tag{4.10}$$

For given pressure ratio p_1/p_0 and given α, (4.10) specifies the speed of propagation of A shocks. To describe the structure, we express the left-hand side of (4.7) in terms of α by means of (2.35). We introduce

$$y = \alpha/\alpha_0, \quad M_0^2 = U^2/c_0^2, \quad \eta = x/R_0(3\alpha_0)^{\frac{1}{2}}. \tag{4.11)–(4.13}$$

From (4.8) and (4.9) it follows that, in terms of y, the pressure ratio is

$$\frac{p_1}{p_0} = y_1^{-1}\left\{1 - \frac{\alpha_0}{Q_1}(y_1 - y_1^{-1})\right\}.$$

Substituting this into (4.10) gives to order α_0^2

$$M_0^2 = y_1^{-1}\left\{1 + \frac{\alpha_0}{Q_1}(1 + y_1^{-1})\right\}. \tag{4.14}$$

Using (4.11)–(4.14), we find, upon inserting (4.7) into the left-hand side of (2.35) and doing some algebra,†

$$\frac{(1-y)(y_1-y)(y+C)}{y} = \frac{d^2y}{d\eta^2} + \delta^* \frac{dy}{d\eta}, \tag{4.15}$$

where

$$\delta^* = \frac{\delta \omega_B R_0}{(3\alpha_0)^{\frac{1}{2}} U}.$$

With $R_0 \sim 10^{-3}\,\mathrm{m}$, $U \sim 10^2\,\mathrm{m\,s^{-1}}$, $\delta \sim 10^{-2}$ and $\omega_B \to 10^4\,\mathrm{s^{-1}}$, δ^* is of order 10^{-2} and hence a small parameter, representing the effect of the kind of dissipation involved in (2.35). The constant C in (4.15) is of order α_0:

$$C = \alpha_0/Q_1. \tag{4.16}$$

Equation (4.15) differs only slightly from

$$(1-y)(y_1-y) = \frac{d^2y}{d\eta^2} + \delta^* \frac{dy}{d\eta}, \tag{4.17}$$

derived by van Wijngaarden (1970) for shocks without relative translational motion, and discussed in more detail by Noordzij (1973). The factor $(y+C)/y$ in (4.15) does not make much difference in the region of interest, $y_1 \leqslant y \leqslant 1$, so the features of the solution of (4.15) are the same as those of (4.17): a sharp decrease of y from 1 to y_1, followed by damped oscillations around $y = y_1$. Therefore we shall need only (4.10) in comparing experiment with theory.

† To avoid an unnecessarily complicated expression, we took $Q = Q_1$ in deriving (4.15).

C shocks

Whereas in A shocks friction plays no role, C shocks are formed by a balance between nonlinear steepening and relaxation. This occurs (see (3.8)) only for pressure ratios slightly larger than unity. In these weak waves, the bubbles suffer no appreciable deformation, and we may put both Q and G in (2.34) equal to unity, corresponding to spherical bubbles. Starting from (2.25), the procedure described above for the A shocks leads here to

$$\frac{p_g}{p_0} = \frac{\alpha_0}{\alpha}\left\{1-\alpha^{-1}\int_{-\infty}^{x}\frac{d\alpha^2}{d\zeta}\exp-\left(\frac{x-\zeta}{U\tau'}\right)d\zeta\right\}, \tag{4.18}$$

where τ' is given by (2.24). Equation (4.18) neatly describes the memory effect in the relation between p_g and α as produced by viscous friction. Combination of (4.4) and (4.18) gives

$$\frac{p_g-p}{p_0} = (\alpha_0-\alpha)\left(\frac{\alpha_0-U^2\alpha/c_0^2}{\alpha\alpha_0}\right)-\frac{\alpha_0}{\alpha^2}\int_{-\infty}^{x}\frac{d\alpha^2}{d\zeta}\exp-\left(\frac{x-\zeta}{U\tau'}\right)d\zeta. \tag{4.19}$$

For $x\to\infty$, $p_g = p = p_1$, and $v-u$ vanishes owing to viscous friction. Then (4.9) and (4.19) give simply

$$U^2/c_0^2 = p_1/p_0, \tag{4.20}$$

an expression found by Campbell & Pitcher (1958), who were concerned with shock waves in which $v = u$ everywhere (i.e. $\tau' = 0$). Inserting (4.19) in (2.35), and using, apart from (4.11)–(4.13), the parameter

$$\epsilon = R_0/[U\tau'(3\alpha_0)^{\frac{1}{2}}], \tag{4.21}$$

we finally obtain

$$(1-y)(M_0^{-2}-y)-\alpha_0(yM_0^2)^{-1}\int_{-\infty}^{\eta}\frac{dy^2}{d\eta'}\exp\left[-\epsilon(\eta-\eta')\right]d\eta' = \frac{d^2y}{d\eta^2}+\delta^*\frac{dy}{d\eta}. \tag{4.22}$$

The parameter ϵ in the integral term is zero in the case of no relative motion, and infinite in the case of zero viscosity. In the experiments of §6, ϵ is of order 10^{-2}. For the purpose of finding the structure of waves in which nonlinear steepening is everywhere balanced by relaxation, we stretch the η scale to

$$\xi = \epsilon\eta. \tag{4.23}$$

Inserting this into (4.22),

$$(1-y)(M_0^{-2}-y)-\alpha_0(yM_0^2)^{-1}\int_{-\infty}^{\xi}\frac{dy^2}{d\xi'}\exp-(\xi-\xi')\,d\xi' = \epsilon^2\frac{d^2y}{d\xi^2}+\delta^*\epsilon\frac{dy}{d\xi}. \tag{4.24}$$

For $\epsilon\to 0$, the right-hand side vanishes, and the equation describes a transition in which nonlinear steepening is everywhere resisted by relaxation. In §3 we found that such a transition is possible only if

$$M_0^2 = p_1/p_0 \leqslant 1+2\alpha_0. \tag{4.25}$$

Since y lies between unity and M_0^{-2}, $(1-y)$ and $(M_0^{-2}-y)$ are of order α_0 in these waves; and, to order α_0^3, we may simplify (4.24) to

$$(1-y)(M_0^{-2}-y)-2\alpha_0\int_{-\infty}^{\xi}\frac{dy}{d\xi'}\exp\left[-(\xi-\xi')\right]d\xi' = 0. \tag{4.26}$$

When we introduce

$$y = \tfrac{1}{2}\{(1+M_0^{-2})+\psi(1-M_0^{-2})\}, \quad \lambda = 2\alpha_0/(M_0^2-1), \qquad (4.27), (4.28)$$

and require that $\psi = 0$ (half way between $y = 1$ and $y = M_0^{-2}$) at $\xi = 0$,

$$(1-\psi)^{1-\lambda}(1+\psi)^{1+\lambda} = \exp\{-\xi\}. \qquad (4.29)$$

For $(1-\lambda) \leqslant 0$, which amounts to (4.25) (from (4.28)), this represents a wave profile in which ψ decreases smoothly from 1 to -1, y consequently from 1 to M_0^{-2}. From (4.4) and (4.27) the dimensionless pressure p/p_0 is related to ψ by

$$p/p_0 = \tfrac{1}{2}\{(1+M_0^2)+\psi(1-M_0^2)\}. \qquad (4.30)$$

The dimensionless pressure rises from 1 to $\frac{1}{2}(1+M_0^2)$ over a distance which is, in terms of ξ, a few times (2, say) $\lambda - 1$. Using (4.28) and remembering that $2\alpha_0$ can be written as (cf. (3.4)) $c_f^2/c_0^2 - 1$, this is equal to $2(c_f^2 - U^2)/(U^2 - c_0^2)$. The rise of $\frac{1}{2}(1+M_0^2)$ to M_0^2 takes place over a distance $2(\lambda+1)$ or $2(c_f^2 + U^2 - 2c_0^2)/(U^2 - c_0^2)$. The overall thickness d_C, say, in terms of the physical distance $U\tau\xi$, is therefore

$$d_C = \frac{4U\tau(c_f^2 - c_0^2)}{U^2 - c_0^2}, \qquad (4.31)$$

in agreement with the estimate (3.9) of § 3. The number 4 means that a representative thickness d_C is chosen over which the pressure difference $p - p_0$ is 90 % of $p_1 - p_0$. Greater accuracy cannot be achieved in experiments.

B shocks

In these shocks relaxation is effective, but not over the whole profile. The pressure ratio is above $1 + 2\alpha_0$, so that a smooth profile, with diffusion due to relaxation everywhere in balance with compressive steepening, is impossible. What happens is that, on the ξ scale (here based on a representative τ rather than the τ' for spherical bubbles), a discontinuity forms at the front of the wave. This discontinuity is a shock wave of the A type. In front the pressure is p_0, at the back p^*, say. There a region, where compressive steepening is balanced by dispersion (the front shock), is succeeded by one where it is balanced by relaxation. In the transition region, the three mechanisms are comparable in importance. A theoretical estimate for p^* can be made in various ways, one of which is as follows. In the front shock, relaxation is unimportant and its propagation velocity must obey, from (4.10),

$$\frac{U^2}{c_f^2} = \frac{p^*}{p_0}\left[1 - \alpha_0\left\{2 - Q_*^{-1}\left(1 + \frac{p_0}{p^*}\right)\right\}\right].$$

The pressure ratio p_1/p_0 follows from conservation of mass and momentum of the whole wave; and just as for the C shocks, it is given by (4.20), resulting, with the aid of (3.4), in

$$\frac{p_1}{p_0} = \frac{p^*}{p_0}\left\{1 + \alpha_0 Q_*^{-1}\left(1 + \frac{p_0}{p^*}\right)\right\}. \qquad (4.32)$$

The pressure recordings (discussed in § 6) give $p - p_0$ relative to the pressure jump $p_1 - p_0$. From (4.32), the theoretical expression for this quantity is

$$\frac{p^*/p_0 - 1}{p_1/p_0 - 1} = 1 - Q_*^{-1}\alpha_0\frac{p_1/p_0 + 1}{p_1/p_0 - 1}. \qquad (4.33)$$

It is easily verified that, for spherical bubbles ($Q = 1$), p^* becomes equal to p_0 to order α_0^2 when $p_1/p_0 = 1+2\alpha_0$, which is the threshold for the existence of C waves. For slightly deformed bubbles, we first estimate the axis ratio χ, and subsequently determine We for this estimate (with help of Moore 1965). Substitution into (4.5) gives the relative velocity $v-u$ used to calculate We. In general this is different from the assumed We. The procedure starts again with a new We. In this way, the value of Q^* can be found after a few iterations.

The y^* value of y, associated with p^* is

$$y^* = y_1 + \alpha_0 O_*^{-1}(1+y_1), \tag{4.34}$$

from (4.4), (4.20) and (4.26). In the region $y^* < y \leqslant 1$, relative motion is not resisted by viscous friction; and the analysis carried out for the A shocks leads to the analogous result

$$\frac{(1-y)(y^*-y)(y+C)}{y} = \frac{d^2y}{d\eta^2} + \delta^* \frac{dy}{d\eta}. \tag{4.35}$$

The equilibrium points are $y = 1$ *and* $y = y^*$. Equation (4.35) is of the same type as (4.15) for the A shock. More interesting is the remainder of the wave, which is governed by the balance between nonlinear steepening and diffusion by relaxation. For spherical bubbles, the analysis of this would be as for the C shocks, but it is anticipated that for the pressure ratios involved here the bubbles are deformed; so it is hard to obtain an exact description. For a theoretical estimate of the width of this part of the wave, we represent the continuously varying form by a representative constant form over the whole relaxation zone. For this, we take the equilibrium form of the bubble at $p = p^*$, for which Q_* is obtained as described above. Associated with this form is an axis ratio χ^*, for which the drag can be calculated from (2.18). This procedure will overestimate the effect of deformation, because the chosen constant form represents the largest deformation. Eventually, at the tail of the wave where $v-u$ vanishes, the bubbles are spherical again. For the bubble form at $p = p^*$, the quantity $G_*(\chi)/Q_*(\chi)$, substituted into (2.27), gives us a representative relaxation time τ.

With ϵ and ξ as defined in (4.21) and (4.23), we find for $\epsilon \to 0$ (in the same way as (4.24) is obtained for C shocks)

$$(1-y)(M_0^{-2}-y) - \frac{\alpha_0}{Q_*}(yM_0^2)^{-1}\int_{-\infty}^{\xi} \frac{dy^2}{d\xi'} \exp -(\xi-\xi')\, d\xi' = 0. \tag{4.36}$$

The front shock is, on the ξ scale, a discontinuity. We take $\xi = 0$ there, and write in the relaxation zone $\xi \geqslant 0$

$$y = 1 + \{(y_1 - 1) + f(\xi)\} I(\xi), \tag{4.37}$$

where $I(\xi)$ is Heaviside's unit step function. With a view to (4.34) the function f is of order α_0. We insert (4.37) into (4.36) and neglect terms of order α_0^2. Then the integral term yields $\{\alpha_0/Q_*\}(y_1^2-1)\exp\{-\xi\}$, and

$$f = \{\alpha_0/Q_*\}(1+y_1)\exp\{-\xi\}.$$

Together with (4.37), for $\xi \geqslant 0$, this gives

$$y = y_1 + \alpha_0 Q_*^{-1}(1+y_1)\exp\{-\xi\}. \tag{4.38}$$

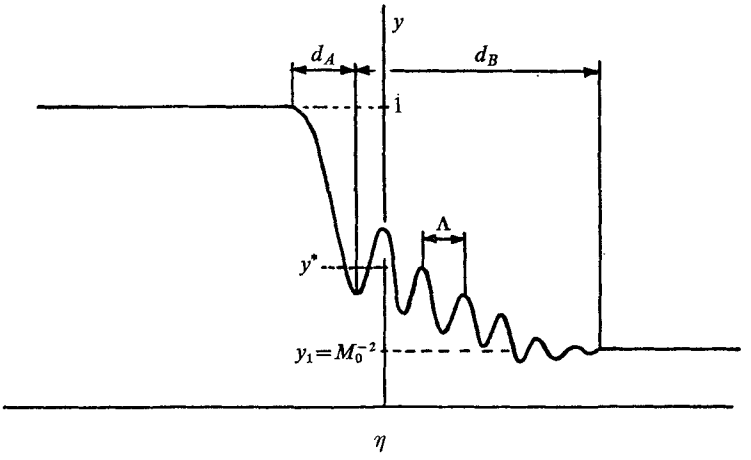

FIGURE 3. Profile of the shock waves in region B, in terms of y as a function of η. Important quantities, such as d_A, wavelength Λ, y^* and d_B, are indicated.

At the discontinuity $\xi = 0$, this gives

$$y^* = y_1 + \alpha_0 Q_*^{-1}(1 + y_1),$$

which supports the independently obtained estimate (4.34). Since y_1^{-1} equals M_0^2 or (from (4.20)) p_1/p_0, with (4.4) we may also write (4.38) in the form

$$\frac{p/p_0 - 1}{p_1/p_0 - 1} = 1 - \alpha_0 Q_*^{-1} \frac{p_1/p_0 + 1}{p_1/p_0 - 1} \exp\{-\xi\}. \tag{4.39}$$

The thickness of the relaxation zone in B shock waves (d_B, say), is therefore a few times $U\tau$,

$$d_B \simeq U\tau. \tag{4.40}$$

The various quantities of interest for B shocks are shown in figure 3.

5. Summary of results for isothermal and adiabatic bubbles: effect of thermal relaxation

When D is the diffusivity of heat in air, $(Dt)^{\frac{1}{2}}$ measures how deep heat penetrates into a bubble by conduction. The relaxation time we found is τ, which is of order 10^{-2} s. With $D = 18 \times 10^{-6}\,\mathrm{m^2\,s^{-1}}$, $(D\tau)^{\frac{1}{2}}$ is about 4×10^{-4} m for this value of τ, which is appreciably smaller than the bubble radii occurring in the experiments ($\sim$ 1 mm). In other words, the thermal relaxation time is longer than the viscous relaxation time τ. Thermally the processes are therefore most likely to occur adiabatically. In that case, $p_g \sim \rho_g^\gamma$ (where $\gamma = 1{\cdot}4$ is the ratio between specific heats of the gas in the bubbles, in our case air). All the calculations can be carried out with this relation as well. Because the isothermal formulae are less complicated, we developed the theory of §§ 2–4 for isothermal bubbles. We now summarize these results, and give the corresponding expressions for adiabatic bubbles.

A shocks

$$M_0^2 = \begin{cases} p_1/p_0\{1+\alpha_0 Q_1^{-1}(1+p_0/p_1)\} & \text{(isothermal)}, \quad (5.1) \\ \dfrac{p_1/p_0-1}{1-(p_0/p_1)^{1/\gamma}}\{1+\alpha_0 Q_1^{-1}(1+(p_0/p_1)^{1/\gamma}\} & \text{(adiabatic)}. \quad (5.2) \end{cases}$$

The speed of the shock wave, in which the bubbles eventually move with the fluid, is

$$M_0^2 = \begin{cases} p_1/p_0 & \text{(isothermal)}, \quad (5.3) \\ \dfrac{p_1/p_0-1}{1-(p_0/p_1)^{1/\gamma}} & \text{(adiabatic)}. \quad (5.4) \end{cases}$$

B shocks

$$F = \frac{p^*/p_0-1}{p_1/p_0-1} = \begin{cases} 1-\alpha_0 Q_*^{-1}\dfrac{p_1/p_0+1}{p_1/p_0-1} & \text{(isothermal)}, \quad (5.5) \\ 1-\gamma\alpha_0 Q_*^{-1}\dfrac{1+(p_0/p_1)^{1/\gamma}}{\gamma-M_0^2(p_0/p_1)^{(\gamma+1)/\gamma}} & \text{(adiabatic)}. \quad (5.6) \end{cases}$$

$$d_B \simeq U\tau. \quad (5.7)$$

C shocks

C shocks occur when

$$p_1/p_0 < \begin{cases} 1+2\alpha_0 & \text{(isothermal)}, \quad (5.8) \\ 1+4\gamma\alpha_0/(\gamma+1) & \text{(adiabatic)}. \quad (5.9) \end{cases}$$

The profile is given by

$$\frac{p/p_0-1}{p_1/p_0-1} = \tfrac{1}{2}(1-\psi), \quad (5.10)$$

where

$$(1-\psi)^{\lambda-1}(1+\psi)^{\lambda+1} = \exp\{-x/(U\tau')\}, \quad (5.11)$$

and

$$\lambda = \begin{cases} 2\alpha_0/(M_0^2-1) & \text{(isothermal)}, \quad (5.12) \\ 2\alpha_0\gamma/(M_0^2-\gamma) & \text{(adiabatic)}. \quad (5.13) \end{cases}$$

The thickness is

$$d_C \simeq \lambda U\tau'. \quad (5.14)$$

From the estimate of the thermal penetration depth made at the beginning of this section, it follows that the thermal relaxation time is longer, but not an order of magnitude so, than the viscous relaxation time. This means that in some of the B and C shocks, thermal relaxation may be effective. To distinguish between thermal and viscous relaxation, it is useful to consider how thermal relaxation works out. Without a complete theory at hand, it is clear that the two velocities of sound occurring in a thermal relaxation theory are the isothermal sound speed c_0 and the adiabatic sound speed $\gamma^{\frac{1}{2}}c_0$.

By analogy with our relaxation theory it appears that smooth profiles occur below a pressure ratio equal to the ratio of the squares of these sound speeds, or in the case of air bubbles,

$$p_1/p_0 \leqslant \gamma = 1{\cdot}4. \quad (5.15)$$

This was noticed by Crespo (1969). With viscous relaxation smooth profiles are predicted for pressure ratios as given by (3.8). To make our discussion of the experiments easier, we now give an estimate for the value of $p^*_{\rm ad}$ associated with a thermal relaxation pressure profile. The front part must obey (5.4):

$$\frac{U^2}{c_0^2} = \frac{p^*_{\rm ad}/p_0 - 1}{1-(p_0/p^*_{\rm ad})^{1/\gamma}}.$$

For the whole wave we have

$$U^2/c_0^2 = p_1/p_0,$$

whence

$$\frac{p_1}{p_0} = \frac{p^*_{\rm ad}/p_0 - 1}{1-(p_0/p^*_{\rm ad})^{1/\gamma}}. \tag{5.16}$$

The F valid for a thermal B shock is therefore

$$F_{\rm ad} = \frac{p^*_{\rm ad}/p_0 - 1}{p_1/p_0 - 1}. \tag{5.17}$$

It is easily verified that $p^*_{\rm ad}$ is p_0 for $p_1/p_0 = \gamma$.

6. Experiments compared with theory

The experiments were carried out in a vertically mounted cylindrical tube with inner diameter of $5{\cdot}5 \times 10^{-2}$ m (shown schematically in figure 1). In this Perspex tube, shock waves were generated as described in Noordzij (1973) and van Wijngaarden (1972*b*). The tube was almost completely filled with an aqueous solution of glycerine. The density of the resulting liquid was $1{\cdot}17 \times 10^3\,{\rm kg\,m^{-3}}$, the viscosity $\nu = 7 \times 10^{-6}\,{\rm m^2\,s^{-1}}$, the surface tension $\sigma = 7 \times 10^{-2}\,{\rm N\,m^{-1}}$. By evacuating the air-occupied region, the pressure in the mixture was decreased below atmospheric pressure. Bubbles were supplied through a system of many capillary tubes at the bottom of the tube. In the undisturbed state, these bubbles are locally almost all of the same size. The glycerine was added to keep buoyancy effects as small as possible. When the mixture was at rest at this low pressure, the mean volumetric gas content was determined. The local value of the gas fraction in each experiment follows from this mean value, together with the known isothermal distribution of gas fraction in the undisturbed state. A photograph of the mixture was made, by means of which the bubble size R_0 was determined. After this a step wave was generated at the upper boundary of the mixture by puncturing the seal on the top of the tube, thereby admitting atmospheric pressure in the air region at the top. The profile of the pressure wave passing along the tube was recorded at A, B and C (figure 1), where the distances between the different locations are also given. The wave propagation velocity was also detected at these locations. A record of the profiles was discussed qualitatively (§§2–5). In this section we make a quantitative comparison with theory.

A shocks

A record for this region is shown in figure 4 (plate 2): a steep increase in pressure at the front part of the shock and attenuated waves at the back. This, as well as other pressure records to be shown, represents the pressure as a function of time,

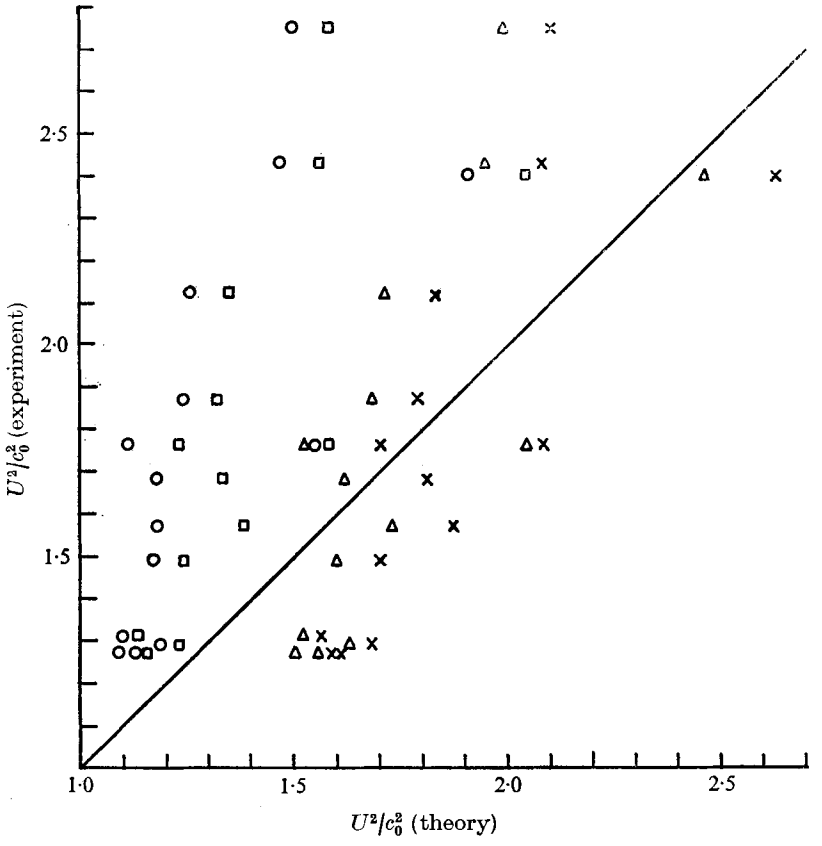

FIGURE 5. Theoretical and experimental values of U^2/c_0^2 in region A. Experiment: ○, isothermal, resisted, (5.3); □, isothermal, not resisted, (5.1); △, adiabatic, resisted, (5.4); ×, adiabatic, not resisted, (5.2). ——, theory.

at a given location. Comparison with theory, where the pressure is given in terms of the space variable x, is possible by the transformation $t = x/U$, where U is for each record the pertinent propagation velocity. From the record in figure 4 (plate 2), shock thickness, wavelength, attenuation of the waves, and the shock strength are determined. These quantities were discussed in Noordzij (1973) and van Wijngaarden (1972*b*), where good agreement with theory was found. In this paper, therefore, we do not pay much attention to these quantities, and we consider mainly relaxation effects. For this reason, it is of interest to decide with which relation for U^2/c_0^2 the experiments agree. For this purpose, we collected the different theoretical and experimental values for U^2/c_0^2 in figure 5. The value for c_0 is given by (2.9). It is the velocity with which waves of infinite wavelength propagate through the mixture. For each experiment, the measured value of U^2, divided by c_0^2, is found to be $(U^2/c_0^2)_{\text{exp}}$ along the vertical axis. The four different theoretical values for the quantity U^2/c_0^2 [(5.1)–(5.4)], at given p_1/p_0 and α_0, are registered along the horizontal axis. When either the isothermal (resisted, not resisted) or adiabatic (resisted, not resisted) theory fits the experiments, the marks representing the pertinent theory are close to the solid line.

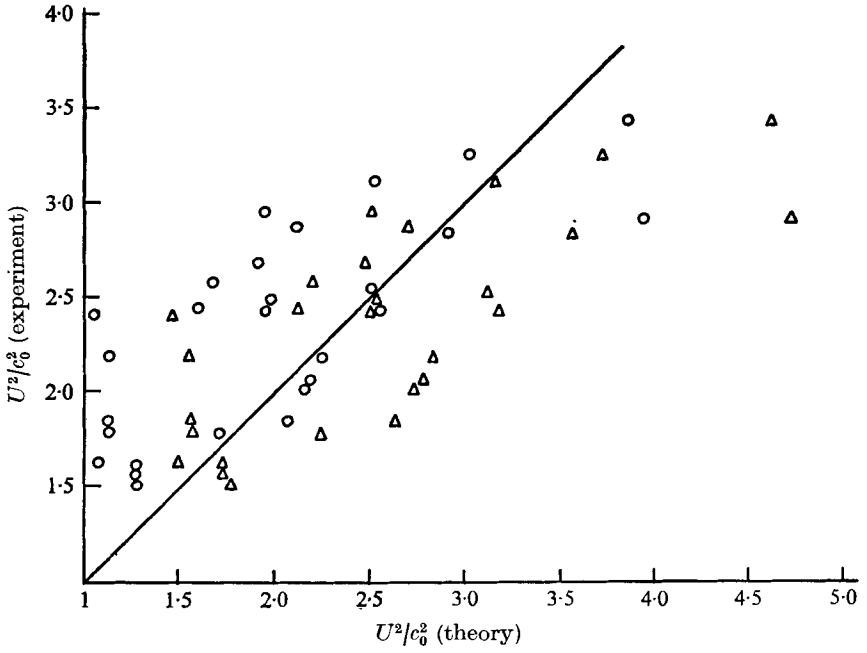

FIGURE 7. Theoretical and experimental values of U^2/c_0^2 in region B. Experiment: ○, isothermal, resisted, (5.3); △, adiabatic, resisted, (5.4). ——, theory.

The conclusion we draw from figure 5 is that the adiabatic marks are definitely closer to the solid line than the isothermal. The difference between the values for U^2/c_0^2 of waves resisted by friction, and waves not so resisted, is (see figure 5) of the order of magnitude of the scatter; so in this respect the experiments provide no verification.

B shocks

The structure of the shock is considerably modified by relaxation, as shown in figure 6 (plate 3). Again there is a steep increase at the front part; but now it is followed by a smooth rise of the pressure, together with small amplitude oscillations, up to the equilibrium pressure. From this record shock thickness, wavelength, typical length for the smooth profile, p^* and the shock strength are determined. For B shocks, we are again interested in which relation for U^2/c_0^2 agrees with the experiments. For this purpose, we collect in figure 7 the different theoretical and experimental values for U^2/c_0^2, in analogy to figure 5.

But, in contrast to figure 5, we present here only two of the four values for U^2/c_0^2 (from the discussion of figure 5 about scatter). Because of this, in figure 7 we cease to distinguish between resisted and not resisted. On the other hand, from the discussion in § 3 about region B, when $x/c_f\tau$ exceeds unity, the theory in which nonlinear steepening is resisted by relaxation can be expected to hold. For these reasons, we register in figure 7 the isothermal (resisted) and adiabatic (resisted) values for U^2/c_0^2, according to (5.3) and (5.4), respectively. When either the isothermal or adiabatic theory fits the experiments, the marks representing

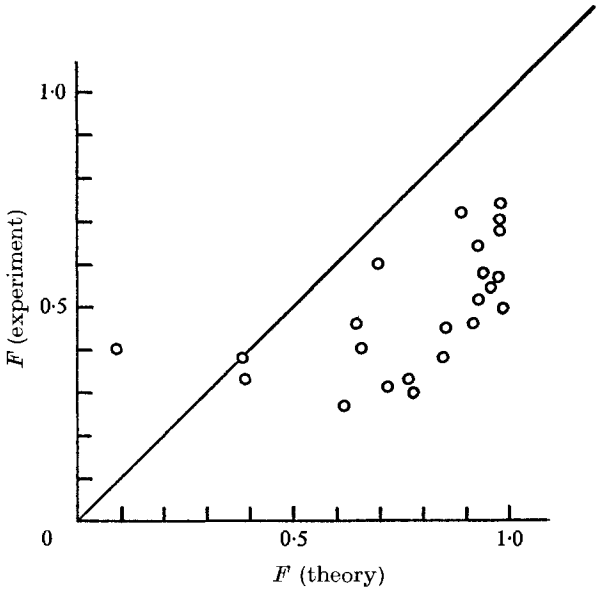

FIGURE 8. Theoretical and experimental values of $F = (p/p_0^* - 1)/(p_1/p_0 - 1)$: ——, theory, (5.6); O, experiment.

the pertinent theory are close to the solid line. However, from figure 7 no clear conclusion can be reached as to which theory applies (but see the remarks on thermal relaxation, below). To compare the theoretical and experimental results for p^* and d_B, we make an estimate for the deformation expressed by χ. In § 4 we took as representative the value χ^* at $p = p^*$. For given α_0, p_1/p_0, χ^* and F, the relative velocity $v - u$ is, from (4.4) and (5.5),

$$\frac{v-u}{U} = \frac{\alpha_0 Q_*^{-1}}{1-(1-p_0/p_1)F}[1-\{1-F(1-p_0/p_1)\}^2]. \tag{6.1}$$

We could as well use here the corresponding adiabatic relation. The relation (6.1), together with (2.16), (2.17), (2.21) and the experimental values for U, α_0, p_1/p_0 and F, enable one to calculate the relative velocity at $p = p^*$ and the corresponding values for We^*, Re^* and χ^*. The experimental data and these quantities are collected in table 1. It turns out that We^* is less than 4 in 26 out of 35 experiments, and less than 1·7 in 19 of these. We may therefore conclude that the theory of §§ 2–5, which excludes Weber numbers greater than 3·75, is applicable. We start by considering the quantity F, as defined by (5.6), which determines the situation of p^*. The theoretical values F_{th} and the experimental values are given in table 1; and those for which $We^* < 3{\cdot}75$ appear in figure 8. This figure shows that the theoretical values for F are systematically above the corresponding experimental ones.

To illustrate this in another way, we plot the experimental values for given α_0 as a function of p_1/p_0 in figure 9. The theoretical curve is for (5.6) and $Q = 1$. At low pressure ratios, the deformation of the bubbles is small, whereas for p_1/p_0 above 1·8 the theoretical values of F are already near unity, and not very

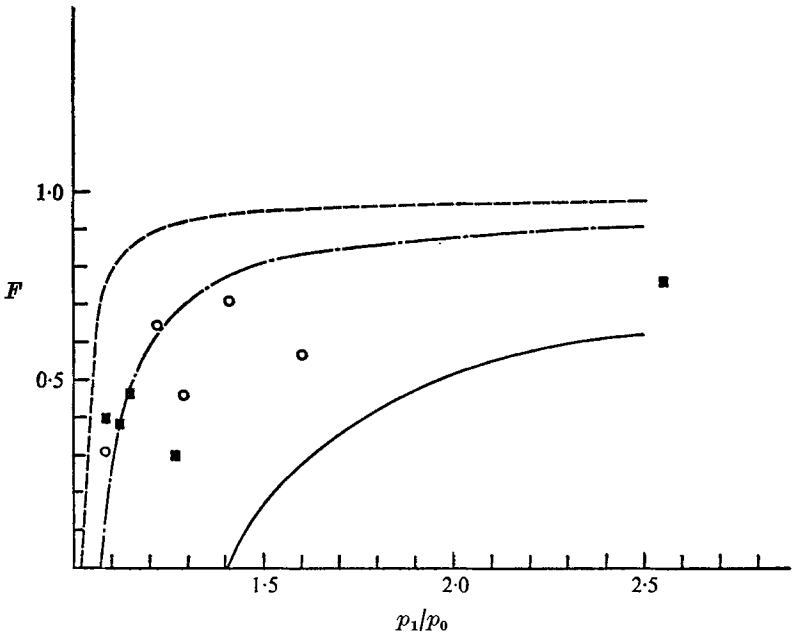

FIGURE 9. F, (5.6), as a function of p_1/p_0, with α_0 a parameter. $\alpha_0 = 0{\cdot}87 \times 10^{-2}$: – – – –, theory; ○, experiment. $\alpha = 3{\cdot}1 \times 10^{-2}$: –·–·–, theory; ■, experiment. ——, $(p^*_{ad}/p_0 - 1)/(p_1/p_0 - 1)$ from thermal relaxation, (5.17).

sensitive to variations in either α_0 or Q. The curve for $Q = 1$ is therefore sufficient to compare theory with experiment. In figure 9 we also draw the curve for thermal relaxation, according to (5.16) and (5.17). It is evident that the experimental data are closer to the line for viscous than to that for thermal relaxation. For large pressure ratios, this is less clear, because the theoretical curves tend to run close to each other. Figure 9 illustrates that, for B shocks, thermal relaxation is noticeable, shown by the deviation of the experimental data from the theoretical line based upon relaxation due to viscous friction.

Another quantity of interest is the length d_B. The theoretical value is of order $U\tau$, τ being given by (2.27). The values for Q_* and G_* can be obtained for each χ^* from (2.21) and (2.19). Although G rises rather sharply with χ, so does Q with the interesting result that their ratio differs less than 5 % from 1 for $\chi \leqslant 1{\cdot}7$ and less than 10 % for $\chi < 2$. Because for the bulk of the experiments of table 1 $\chi^* < 1{\cdot}7$, one may set $Q_*/G_* = 1$ in (2.27) when comparing theoretical with the experimental values of d_B. We define d_B as the distance over which $p_1 - p$ rises from $p_1 - p^*$ to 10 % of $p_1 - p_0$, in analogy with the definition of d_C (4.25). It follows from (4.39) then that

$$\frac{d_B/U\tau}{\ln\{10(1-F)\}} = 1. \tag{6.2}$$

The experimental values of the left-hand side of (6.2), which we call K, are given in table 1. The mean value of K for those experiments for which $\chi^* < 1{\cdot}7$ is $K = 0{\cdot}68$. In figure 10 the distribution function for K is given. The standard

	p_1/p_0	β_0 (%)	R_0 (mm)	U_{exp} (ms^{-1})	F_{exp}	F_{th}	$v-u$ (ms^{-1})	We	Re	χ	K
1	1·07	1·22	1·03	156	0·27	0·62	0·08	0·25	25	1·05	0·69
2	1·07	2·94	1·18	70	0·40	0·09	0·12	0·60	42	1·10	0·36
3	1·08	0·97	0·94	143	0·31	0·72	0·06	0·11	16	1·00	0·86
4	1·11	1·43	1·05	115	0·60	0·70	0·17	1·00	51	1·20	0·90
5	1·12	1·72	1·09	90	0·40	0·66	0·14	0·60	44	1·10	0·61
6	1·12	3·41	1·21	66	0·38	0·38	0·17	1·00	59	1·20	0·41
7	1·14	1·47	1·01	119	0·33	0·77	0·17	0·60	50	1·20	0·83
8	1·14	2·43	1·10	94	0·27	0·61	0·16	1·00	50	1·20	0·86
9	1·15	2·71	1·15	79	0·46	0·65	0·20	1·50	70	1·30	0·48
10	1·15	4·68	1·21	55	0·33	0·39	0·19	1·50	66	1·30	0·46
11	1·18	1·12	1·00	111	0·45	0·86	0·17	1·00	49	1·20	0·96
12	1·19	1·58	1·31	85	0·72	0·89	0·23	2·35	87	1·70	0·87
13	1·21	0·69	0·91	167	0·46	0·92	0·18	1·00	47	1·20	0·93
14	1·23	0·81	0·95	119	0·64	0·93	0·22	1·50	59	1·30	1·30
15	1·27	3·52	1·19	69	0·30	0·78	0·22	2·00	76	1·50	0·56
16	1·28	2·29	1·22	85	0·38	0·85	0·22	2·00	77	1·50	0·40
17	1·29	0·81	1·09	139	0·46	0·94	0·20	1·50	64	1·30	0·52
18	1·41	0·87	1·19	116	0·70	0·97	0·24	2·35	83	1·70	0·41
19	1·42	2·19	1·28	85	0·57	0·94	0·27	3·10	99	2·40	0·38
20	1·42	3·03	1·45	69	0·52	0·93	0·26	3·20	107	2·50	0·23
21	1·6	0·88	1·03	143	0·57	0·97	0·28	2·00	76	1·50	0·47
22	1·61	1·90	1·25	122	0·57	0·97	0·29	3·50	105	3·20	0·38
23	1·61	2·76	1·38	88	0·56	0·96	0·29	3·55	110	3·30	0·37
24	1·96	2·19	1·36	100	0·69	0·98	0·32	3·75	116	4·00	0·48
25	1·97	2·86	1·48	79	0·55	—	—	—	—	> 4	0·29
26	1·99	1·12	1·08	128	0·50	0·99	0·30	3·20	92	2·50	0 56
27	2·51	1·43	1·11	93	0·74	0·99	0·30	3·75	98	4·00	0·41
28	2·54	2·39	1·29	79	0·82	—	—	—	—	> 4	0·41
29	2·56	3·49	1·39	58	0·76	—	—	—	—	> 4	0·29
30	2·91	1·72	1·19	83	0·76	—	—	—	—	> 4	0·22
31	3·00	3·64	1·54	58	0·79	—	—	—	—	> 4	0·15
32	3·04	2·77	1·24	70	0·79	—	—	—	—	> 4	0·29
33	3·83	1·98	1·1	73	0·78	—	—	—	—	> 4	0·34
34	3·87	2·77	1·36	67	0·81	—	—	—	—	> 4	0·42
35	3·96	2·94	1·4	59	0·81	—	—	—	—	> 4	0·40

TABLE 1. Summary of experiments in region *B*

deviation is 0·25. This is of the same order of magnitude as the relative errors involved in the measurements. It therefore appears that the relaxation time deduced from the experiments is smaller than that predicted by theory.

C shocks

Finally, we consider *C* shocks, in which the profile is smooth and follows from a balance of nonlinear steepening and relaxation. A typical record for the pressure as a function of time is shown in figure 11 (thick line), where the theoretical relation (thin line) for the adiabatic case is also given. This theoretical curve is formed from (5.10), (5.11) and (5.13), using the transformation $t = x/U$. *C* shock waves occur according to the adiabatic theory for pressure ratios given by (5.9), and according to the isothermal theory given by (5.8). If we compare both

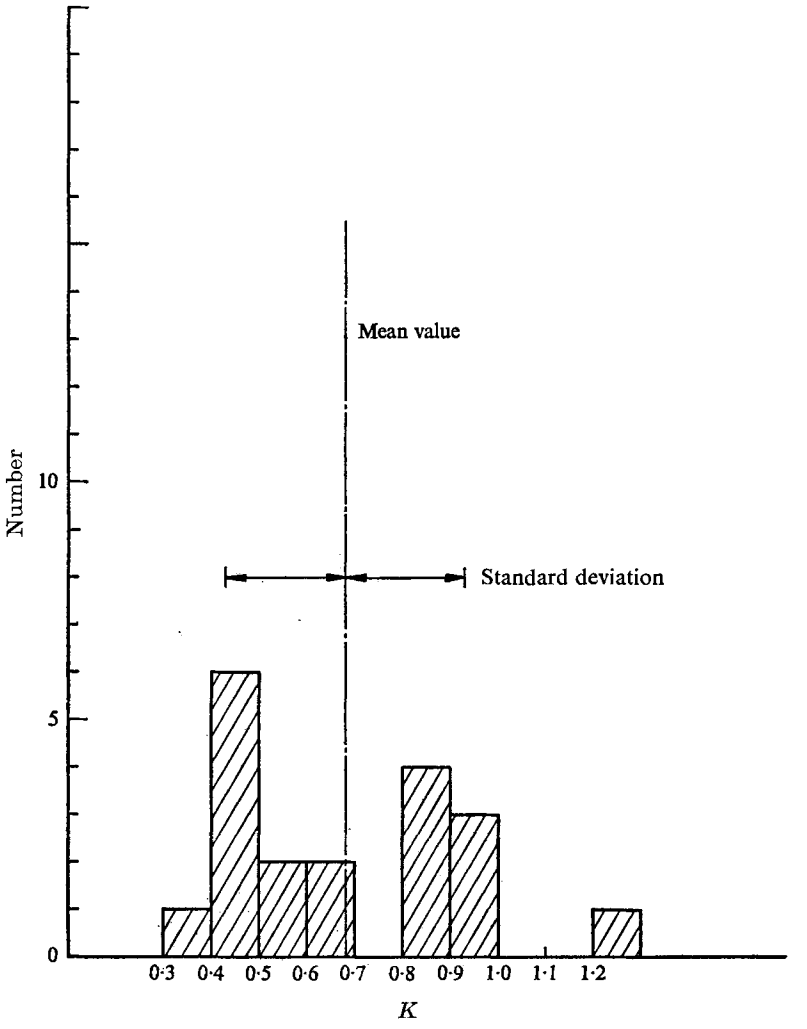

FIGURE 10. Distribution function of K. Mean value is 0·68, standard deviation 0·25. Experiments in which $\chi^* \leqslant 1{\cdot}7$.

limiting values with the experimental values for p_1/p_0 in table 2, for which we observed smooth profiles, it follows that the appearance of smooth profiles answers to the adiabatic relation. For that reason, in figure 11 the adiabatic representation is compared with the experimental curve. The figure shows that the theoretical pressure changes over a distance appreciably longer than the experimental one. However, by changing the timewise variable in the theoretical pressure profile, this curve appears to fit the experimental curve, though with a different relaxation time τ'. Actually, the fit is best with a relaxation time about one half of the theoretical value $R_0^2/18\nu$. The measured pressure profile therefore has the shape predicted, but a smaller relaxation time; this we also found for B shocks (see §7). In table 2 the value for the shock thickness d_C following from (5.14) is given for different experiments. The propagation velocity is not shown in

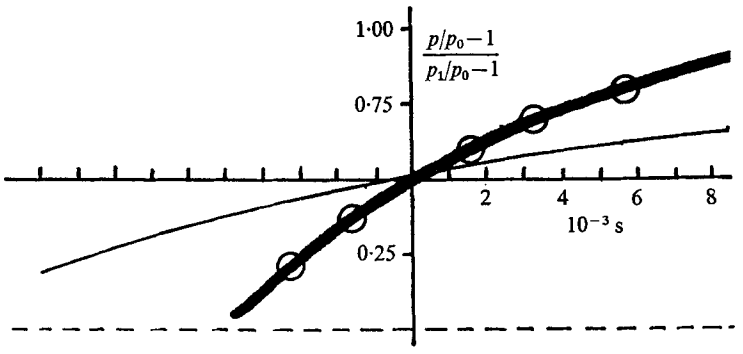

FIGURE 11. ▬▬, $(p/p_0-1)/(p_1p_0-1)$ as a function of t in region C: $p/p_0 = 1{\cdot}08$; $\beta_0 = 3{\cdot}7\times10^{-2}$; $R_0 = 1{\cdot}17\times10^{-3}$ m; $d_C = 2{\cdot}04$ m; $1+4\gamma\alpha_0/(\gamma+1) = 1{\cdot}085$. ——, adiabatic theory (5.9), (5.11), $\tau = 10^{-2}$ s, using transformation $x/U = t$; ○, theoretical values of pressure if τ' is one half of the theoretical value $R_0^2/18\nu$.

$\frac{p_1}{p_0}$	β_0 (%)	$1+2\beta_0$	$1+\frac{4\gamma\beta_0}{\gamma+1}$	R_0 (mm)	$\frac{d_C}{U\tau}\frac{M_0^2-\gamma}{4\alpha_0}$
1·06	2·58	1·052	1·061	1·13	1·09
1·06	3·77	1·075	1·088	1·19	0·81
1·08	2·32	1·046	1·054	1·16	1·30
1·08	3·67	1·073	1·085	1·17	1·30
1·13	4·07	1·081	1·094	1·15	1·64

TABLE 2. Summary of experiments in region C

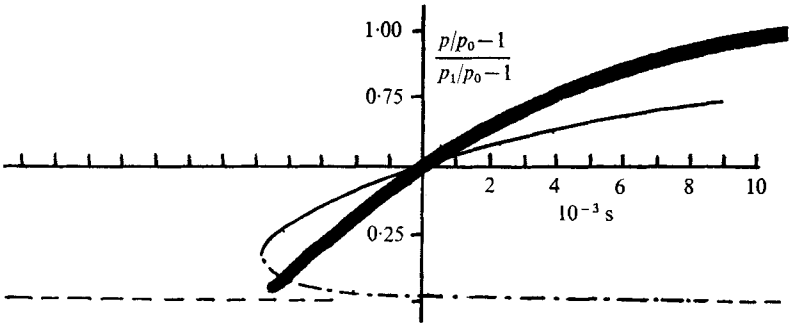

FIGURE 12. ▬▬, pressure record, as in figure 11. ——, theory (turns back, indicating a weak front shock not observed in the experiment).

this table, because the profile was not steep enough to permit measurement of U. $d_C/U\tau$ does not depend on U; d/U is measured directly, because the experiments have the pressure as a function of the timewise variable x/U. In figure 12 another record of a C shock is presented (experiment 5, table 2).

According to the theory, a thin front shock of small strength should appear because the pressure ratio $p_1/p_0 > 1+4\gamma\alpha_0/(\gamma+1)$. But here it is hard to decide from the figure whether or not a front shock is present (in other words, whether

the shock is of B or C type). In all other cases, it is clear that, for pressure ratios p_1/p_0 between γ (see (5.15)) and $1+4\gamma\alpha_0/(\gamma+1)$, only B shocks are found experimentally. We consider this substantial support for our theory (which is based on relaxation connected with relative motion).

7. Discussion

The theory predicts effects of relaxation on the speed of propagation and on the form of the pressure profile. The experiments do not allow one to measure the influence on the former, but demonstrate the existence of definite effects on the latter. This involves, in the case of B shocks, a front shock with pressure ratio p^*/p_0. The theoretical value for p^* is obtained from matching a dispersion-dominated with a relaxation-dominated shock. p^* is in the transition region between these. This region is ignored in our theory, which therefore provides only an approximate value for p^*. In view of this and of what is said about thermal relaxation in § 6, we may say that qualitatively the experiments support the part of the theory about p^*.

In § 6 we found a smaller relaxation time for B and C shocks than was predicted. Actually, the mean value of K in figure 10 implies a relaxation time of about one half the theoretical value $R_0^2/18\nu$. Calculating χ^*, we decided that, for the relatively low χ^* in the experiments, the value of τ for spherical bubbles is applicable. There are several reasons for scatter in the experimental values for K in figure 10. Experimental errors are involved in the measurement of R_0 (about 20 %), in determining the values of d_B and d_C from the oscilloscope recordings (about 10 %). Systematic differences between theory and experiment may be explained by a number of effects we left out of the theory.

(i) *Finite Reynolds number.* In determining the resistance of the bubbles, no correction is made for this. For steady flow such a correction was calculated by Moore (1965); but it is illegitimate to apply it to unsteady flow.

(ii) *Deformation asymmetrical with respect to fore and aft, symmetrical with respect to the direction of relative velocity.* If the potential for the relative motion is ϕ, then this deformation stems from the $\rho\,\partial\phi/\partial t$ in Bernoulli's equation for the pressure. The symmetrical term $\frac{1}{2}\rho|\nabla\phi|^2$ leads to the oblate-ellipsoidal form, which is accounted for. The magnitude of the former term relative to the latter is

$$R\{\partial/\partial t\,(v-u)\}/(v-u)^2.$$

In the relaxation zones, B and C shocks, $\partial/\partial t \sim \tau^{-1}$, and using (2.27), the above ratio is seen to be of order Re^{-1} and therefore small. In A shocks, on the other hand, where $\partial/\partial t$ is of order U/d_A, this ratio is often comparable with unity. We have not made an attempt to estimate the effect of (i) and (ii). If this proved possible, it would require much more theoretical work. Here we merely remark that, alone or in combination, they could cause a systematic difference between the observed and calculated relaxation time.

(iii) *Influence of gravity.* First, this gives rise to buoyancy and a non-zero velocity of the bubbles prior to the passage of a pressure wave. In magnitude this velocity is of order $0{\cdot}2\,\mathrm{m\,s^{-1}}$; and therefore in many of our experiments it is

comparable with the shock-induced velocity, though of opposite sign. For the weak shocks we are dealing with, the relative velocity due to buoyancy is constant during the passage of the shock, and does not for that reason affect its structure. Another question is whether the hydrostatic pressure distribution that exists in the undisturbed mixture might affect the structure of the shock in a significant way. Fortunately, this turns out not to be the case. As might be expected, the hydrostatic pressure distribution found by our experiments modifies the propagation velocity. But for comparison of theory with experiments, to a sufficient level of accuracy the local values for p_0 and β_0 can be used, and no correction for gravity on the structure needs to be carried through. For, for present purposes, we may disregard the effects of dispersion, attenuation and relative translational motion of the bubbles. We consider a pressure disturbance $\bar{p}$ propagating in an undisturbed region with a hydrostatic pressure distribution. The disturbance is defined as the difference between the local and the undisturbed pressure:

$$\bar{p} = p - p_0 \quad \text{where} \quad \bar{p}/p_0 \ll 1.$$

With this we find from the continuity and momentum equations that the disturbance obeys

$$\frac{\partial \bar{p}}{\partial t} + c_0 \frac{\partial \bar{p}}{\partial x} + c_0 \frac{\bar{p}}{p_0} \frac{\partial \bar{p}}{\partial x} + \frac{\rho_f g c_0}{2 p_0} \bar{p} = 0 \tag{7.1}$$

(see the appendix).

In the experiments, a pressure profile was measured at a particular location along the shock tube as a function of time. The theory of §4, with the results of which the measurements are compared, deals with travelling waves described in terms of a moving co-ordinate $x' = x + Ut$. The shock velocity U is expressed in local quantities p_0 and c_0. The error introduced by neglecting gravity can therefore be estimated by calculation of the effect of gravity over the width $U\tau$ of the shock. The effect of gravity appears in the first place through the dependence of c_0 on x, since

$$c_0 = c_{00}(1 + \rho_f g x / p_{00}), \tag{7.2}$$

where c_{00} and p_{00} are constant reference values. Further gravity gives rise to the last term on the left-hand side of (7.1). The nonlinear term $c_0 \bar{p}/p_0 \, \partial \bar{p}/\partial x$ steepens the wave and leads, as was discussed before, combined with a diffusion term on the right-hand side of (7.1), to a constant profile, in the absence of gravity.

The role of the nonlinear term being understood, we may estimate the effect of gravity by considering a linear wave. Consider first

$$\frac{\partial \bar{p}}{\partial t} + c_{00} \frac{\partial \bar{p}}{\partial x} + \frac{\rho_f g c_0}{2 p_0} \bar{p} = 0. \tag{7.3}$$

The relevant solution is a wave travelling with speed c_{00} and attenuated by the factor $\exp\{-(\rho_f g x)/(2p_{00})\}$. The maximum wave thickness occurring in region C is of order $U\tau$. Numerically this is of the order of 1 m. For $p_{00} = 10^5 \,\mathrm{N\,m^{-2}}$ and $U\tau = 1$ m, the exponential is 0·95. Neglecting this attenuation therefore introduces a relative error of about 5 %, which, in view of the experimental accuracy, is negligible. Next we consider the effect of the depencence of c_0 on x:

$$\frac{\partial \bar{p}}{\partial t} + c_{00}\left(1 + \frac{\rho_f g x}{p_{00}}\right) \frac{\partial \bar{p}}{\partial x} = 0. \tag{7.4}$$

This indicates a stretching of the wave. Two wavelets at distance ∇ at $t = 0$ are at a distance $\nabla(1+\rho_f g c_0 t/p_0)$ at t. The longest time, again in region C, necessary for a wave to pass an observer is the relaxation time τ. The quantity $\rho_f g c_0 \tau/p_0$ ranges from 0·05 to 0·10 at most. From these estimates, we conclude that comparison of our experimental data with the theory of §4 justifies our conclusions.

8. Conclusion

This paper was inspired by observing a gradual change in the profile of a shock wave passing through a bubbly liquid. A theory was developed which takes into account the motion of the bubbles relative to the liquid. The theory predicts effects on both wave speed and wave profile: the effect on speed is so small that it was not possible to measure it; the effects on the profile could be measured. The experiments gave fair support for stating that the changes in profile are caused by the relaxation mechanism associated with (initially generated and eventually resisted) motion of the bubbles relative to the liquid.

Some remarks can be made about future work. It seems advisable to use smaller bubbles than the ones produced in our experiments. This leads to smaller Weber numbers, and less deviation from the spherical shape. Also, the effect of §7 (ii) becomes less important. Another improvement might be to use gases with smaller heat diffusivity than air. This would avoid thermal relaxation, and enable one to obtain more accurate data for p^*.

This paper is based on part of a Ph.D. thesis by L. Noordzij at the Twente Institute of Technology, The Netherlands, 1973.

Appendix

To find out in what way a disturbance propagating in one direction is distorted by gravity, we transform the basic equations by introducing

$$\left.\begin{aligned} p &= p_0(1+\epsilon p') \quad \text{for} \quad \epsilon p_0 p' = \bar{p}, \\ \beta &= \beta_0(1+\epsilon\beta') \quad \text{for} \quad \epsilon\beta_0\beta' = \bar{\beta}, \\ u &= \epsilon c_0 \beta_0 u', \quad x = x' c_0 \tau, \quad t = t'\tau. \end{aligned}\right\} \tag{A 1}$$

p_0 and β_0 are given functions of x. From (2.4) and (2.12) neglecting effects of relative translational motion, we have, with $p_g = p$,

$$p\beta/(1-\beta) = \text{const.} \tag{A 2}$$

From this and (2.9) it follows that

$$c_0^2 \beta_0^2 = \text{const.}; \tag{A 3}$$

or, for $\beta_0 \ll 1$,

$$c_0/p_0 = \text{const.} \tag{A 4}$$

From (A 1), it follows that

$$\frac{\partial}{\partial x} = \frac{1}{c_0\tau}\left\{1 - \frac{x}{c_0}\frac{dc_0}{dx}\right\}\frac{\partial}{\partial x'}.$$

With help of (A 4) this can be written as

$$\frac{\partial}{\partial x} = \frac{1}{c_0 \tau}\left\{1 + \frac{\rho_f g x}{p_0}\right\}\frac{\partial}{\partial x'}. \tag{A 5}$$

Further, we define

$$\left\{1 + \frac{\rho_f g x}{p_0}\right\}\frac{\partial}{\partial x'} = \frac{\partial}{\partial \theta}. \tag{A 6}$$

(A 1), (A 5) and (A 6) are introduced in (2.4), (2.5) and (2.12), with $p = p_g$. Terms of order ϵ^2 and lower are retained, terms of order $\beta\epsilon^2$ are discarded. $\rho_f g c_0 \tau / p_0$ is small. For waves of moderate amplitude, travelling in the positive θ direction, we find

$$\frac{\partial p'}{\partial t'} + \frac{\partial p'}{\partial \theta} = \frac{\rho_f g c_0 \tau}{2 p_0} p' - \epsilon p' \frac{\partial p'}{\partial \theta}. \tag{A 7}$$

In the laboratory frame, (A 7) becomes

$$\frac{\partial \bar{p}}{\partial t} + c_0 \frac{\partial \bar{p}}{\partial x} + c_0 \frac{\bar{p}}{p_0}\frac{\partial \bar{p}}{\partial x} + \frac{\rho_f g c_0}{2 p_0}\bar{p} = 0. \tag{A 8}$$

REFERENCES

Campbell, I. J. & Pitcher, A. S. 1958 *Proc. Roy. Soc.* A **243**, 543.

Crespo, A. 1969 *Phys. Fluids*, **12**, 2274.

Lamb, H. 1932 *Hydrodynamics*. Cambridge University Press.

Levich, V. G. 1962 *Physico-chemical Hydrodynamics*. Prentice-Hall.

Lighthill, M. J. 1956 *Surveys in Mechanics* (ed. G. K. Batchelor & R. M. Davies), p. 250. Cambridge University Press.

Marble, F. E. 1970 *Ann. Rev. Fluid Mech.* **2**, 397.

Milne-Thomson, L. M. 1968 *Theoretical Hydrodynamics*. Macmillan.

Moore, D. W. 1963 *J. Fluid Mech.* **16**, 161.

Moore, D. W. 1965 *J. Fluid Mech.* **23**, 749.

Noordzij, L. 1973 *Proc. IUTAM Symp. on Non-steady Flow of Water at High Speeds* (ed. L. I. Sedov & G. Yu-Stepanov), p. 369. Moscow: Nauka.

Ockendon, H. & Spence, D. A. 1969 *J. Fluid Mech.* **39**, 329.

Taylor, G. I. 1954 *Proc. Roy. Soc.* A **225**, 273.

Whitham, G. B. 1959 *Commun. Pure Appl. Math.* **12**, 113.

Wijngaarden, L. van 1968 *J. Fluid Mech.* **33**, 465.

Wijngaarden, L. van 1970 *Appl. Sci. Res.* **22**, 366.

Wijngaarden, L. van 1972*a* *Ann. Rev. Fluid Mech.* **4**, 369.

Wijngaarden, L. van 1972*b* *Heat Mass Transfer*, **6**, 637.

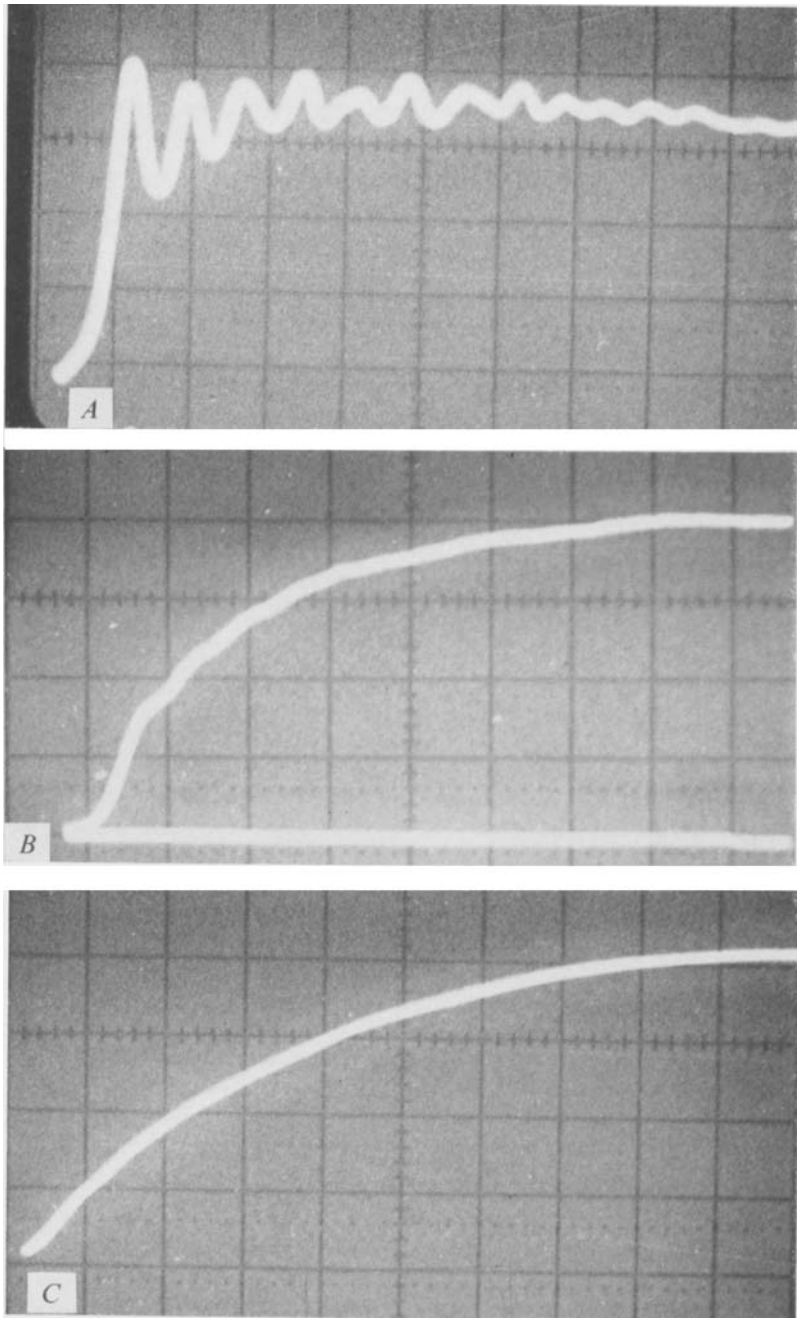

FIGURE 2. Different profiles of the shock wave recorded at places A, B and C, indicated in figure 1.

Region	p_1/p_0	$\beta_0 \times 10^2$	$R_0 \times 10^3$ (m)
A	1·08	3·68	1·27
B	1·07	2·94	1·18
C	1·06	2·58	1·13

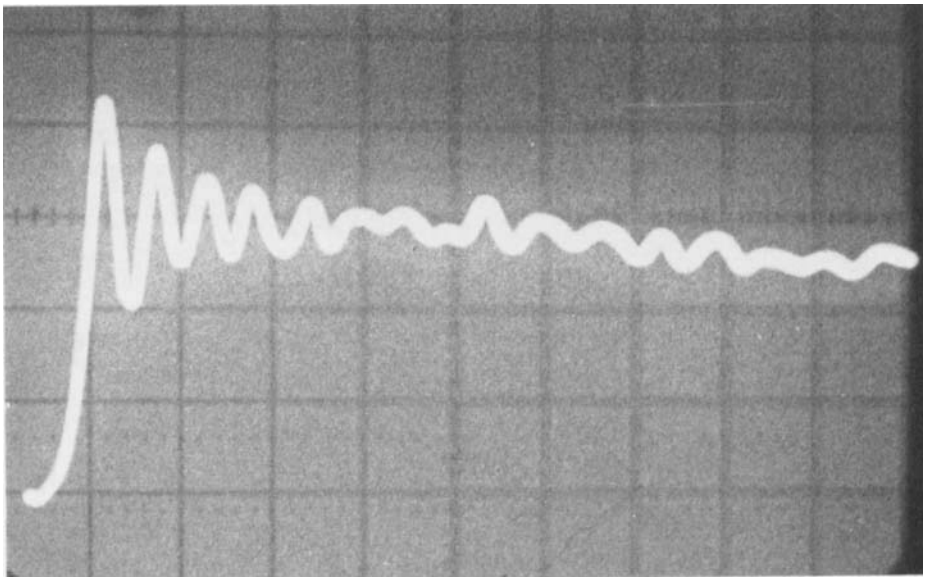

FIGURE 4. Pressure record typical in region A. $p_1/p_0 = 1{\cdot}09$; $\beta_0 = 3{\cdot}28 \times 10^{-2}$; $R_0 = 1{\cdot}32 \times 10^{-3}$ m; $d_A = 7{\cdot}9 \times 10^{-2}$ m; wavelength at back of shock $\Lambda = 6{\cdot}7 \times 10^{-2}$ m.

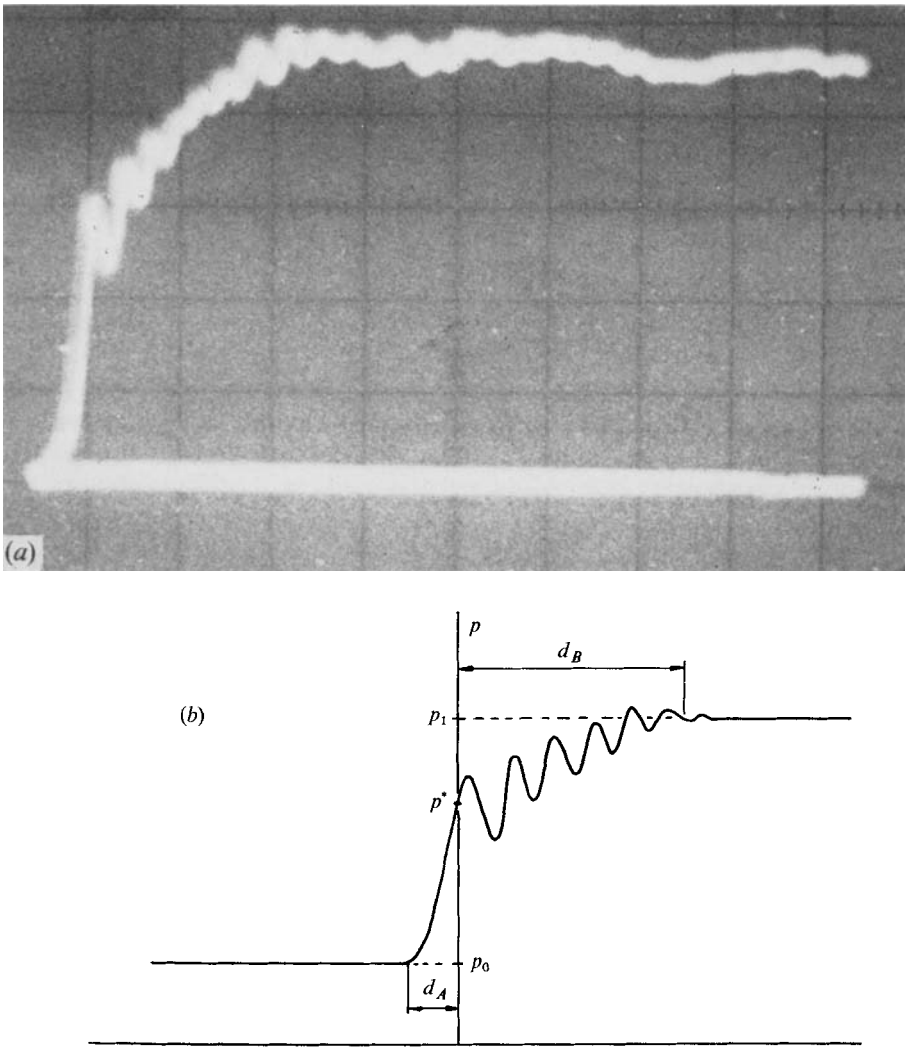

FIGURE 6. Pressure record typical in region B.
$p_1/p_0 = 1{\cdot}42$; $\beta_0 = 2{\cdot}19 \times 10^{-2}$; $R_0 = 1{\cdot}28 \times 10^{-3}$ m; $F_{\exp} = 0{\cdot}57$;
$d_A = 8{\cdot}5 \times 10^{-2}$ m; $\Lambda = 5{\cdot}4 \times 10^{-2}$ m; $d_B = 0{\cdot}357$ m.